Epilepsia, 49(2):269–280, 2008
doi: 10.1111/j.1528-1167.2007.01266.x

FULL-LENGTH ORIGINAL RESEARCH

Synchronization clusters of interictal activity in the lateral temporal cortex of epileptic patients: Intraoperative electrocorticographic analysis

*Guillermo J. Ortega, ‡Liset Menendez de la Prida, *Rafael G. Sola, and †Jesus Pastor

*Neurosurgery and †Clinical Neurophysiology Service, Hospital Universitario La Princesa, Madrid, Spain; and ‡Neurobiology, Research Department, Hospital Ramón y Cajal, Madrid, Spain

SUMMARY

Objective: Drug-resistant temporal lobe epilepsy (TLE) can be treated by tailored surgery guided by electrocorticography (ECoG). Although its value is still controversial, ECoG activity can provide continuous information on intracortical interactions that may be useful to understand the pathophysiology of TLE. The goal of this study is to characterize local interactions in multichannel ECoG recordings of the lateral cortex of TLE patients using three synchronization measures and to link this information with surgical outcome.

Methods: Intraoperative ECoG recordings from 29 TLE patients were obtained using grids of 20 electrodes (4 × 5) covering regions T1, T2, and T3 of the lateral temporal lobe. Linear correlation, mutual information, and phase synchronization were calculated to quantify lateral intracortical interactions. Surrogate data files were generated to test results statistically.

Results: By distributing locally the interactions between the electrodes, we characterized the spatial patterns of ECoG activity. We found clusters of synchronized activity at specific areas of the lateral temporal cortex in most patients. Methodologically, linear correlation and phase synchronization performed better than mutual information for cluster discrimination. ROC analysis suggested that surgical removal of sharply defined synchronization clusters correlated with seizure control.

Conclusions: Our results show that synchronous intraoperative ECoG activity emerges from specific cortical areas that are highly differentiated from the rest of the temporal cortex. This suggests that synchronization analysis could be used to functionally map into the temporal cortex of TLE patients. Moreover, our results suggest that these sites might be involved in the circuits that participate in clinical seizures.

KEY WORDS: ECoG, Temporal lobe epilepsy, Synchronization, Cross-correlation, Clusters.

Drug-resistant temporal lobe epilepsy (TLE) can be treated by tailored surgery guided by electrocorticography (ECoG). Based on this and other presurgical data, the anterior lateral temporal cortex, portions of the amygdala and the hippocampus are commonly excised (Lüders, 1992; Spencer et al., 1984; Sola et al, 2005; Pastor et al, 2005). The goal of surgery is to achieve seizure control. However, while some patients are seizure free or show a significant reduction of seizure activity after surgery, others show no changes or even worsen (Engel, 1993). Therefore, it is important to improve our understanding of the dynamics of cortical activity in the temporal lobe of epileptic patients.

Six theoretical regions have been defined in the presurgical evaluation of epileptic patients (Rosenow and Luders, 2001). The epileptogenic zone, irritative zone, seizure onset zone, epileptogenic lesion, symptomatogenic zone and the functional deficit zone, related with ictal and interictal dynamics in the epileptic process. Prior to a clinical seizure, thousands of neurons in the seizure focus (epileptogenic zone), which is typically located in the hippocampal and parahippocampal regions, undergo

Accepted July 16, 2007; Online Early Publication September 6, 2007.
Address correspondence and reprint requests to Dr. Guillermo J. Ortega, Hospital Universitario de la Princesa, Departamento de Neurocirugía, (planta 7), Diego de León 62, Madrid 28006. Spain, E-mail: ortega@df.uba.ar

Blackwell Publishing, Inc.

depolarization shifts followed by an after-hyperpolarization. As long as this behavior is confined to the seizure focus, there may be no clinical manifestation, even though synchronous activity can be detected as interictal spikes or sharp waves in the EEG or ECoG (irritative zone). As seizure proceeds, the magnitude of the after-hyperpolarization decreases and neurons generate continuous firing of action potentials. The inhibition surrounding the seizure focus weakens and the seizure then spread from the seizure onset zone, corresponding with clinical manifestations (Dichter and Ayala, 1987). This oversimplified picture of the seizure evolution shows that no single area is solely responsible for the clinical seizure, but interplay among them is essential.

Among the several diagnostic tools used to define these regions, intraoperative ECoG analysis has been widely applied as a tool to guide resection. However, its use is still controversial (Schwartz et al., 1997; Keene et al., 2000; McKhann et al., 2000). On one side, visual identification of epileptogenic spikes relies strongly on the expert opinion (Wilson and Emerson, 2002) and disagreement of up to 50% between two experts is not rare (Dümpelmann and Elger, 1999). On the other side, ECoG interictal spikes often derive from the irritative zone, which seems to play no fundamental role in the clinical seizure (Rosenow and Luders, 2001). However, interictal spikes are just an example of the events recorded using intraoperative ECoG. Electrocorticographic signals are generated by the averaged longitudinal current flow of thousands of pyramidal cells in the cortex, organized typically in macrocolumns of 0.3–1 mm wide and 2–4 mm depth (Nunez, 1993). Electrical activity recorded using ECoG arrays can thus give us continuous information on intracortical interactions, even in the absence of interictal spikes (Gray et al., 1989). Previous work has examined the spatial interactions of continuous EEG data, as opposed to discrete spike analysis (Quian Quiroga et al., 2002; Bartolomei et al. 2004). Local increase of coherence during interictal period has been reported in particular regions of the temporal lobe by using ECoG (Towle et al., 1998; Towle et al., 1999). Very recently, the existence of local synchronization during ictal activity has been examined in MEG recordings (Garcia Dominguez et al., 2005). It has also been shown that the seizure onset zone exhibits higher synchronization than any other region, even during the interictal period (Arnhold et al., 1999; Mormann et al., 2000) and that increased synchronization of interictal activity can help to lateralize seizures (Kraskov, 2004).

Here we will apply three well-known synchronization measures commonly used in the analysis of electrophysiological data: the Pearson correlation coefficient, mutual information, and phase synchronization. We aim to characterize local interactions in multichannel ECoG recordings of the lateral cortex of TLE patients. As we will show, interactions do not distribute evenly over the lateral temporal cortex, instead regions of higher synchronization, i.e., synchronization clusters, are typically detected. The patterns of synchronization clusters are very inhomogeneous between different patients, with cases ranging from sharply defined clusters to very distributed synchrony. We will show that the removal of sharply defined synchronization clusters correlate with good surgical outcomes, suggesting that regions of higher interdependences in the lateral cortex might participate in the circuits involved in seizure generation.

Methods

Neurophysiological data

A total of 29 drug-resistant TLE patients, who underwent surgery at the Epilepsy Unit of the Hospital de La Princesa, were included in this study (Table 1). Informed consent and approval by the local ethic committee were always obtained. Patients were evaluated intraoperatively with 4 × 5 subdural electrode grids (interelectrode distance, 1 cm) and a 1 × 8 electrode mesial strip, under low doses of sevoflurane (0.5%) and remifentanyl (0.1 mg/kg/min). During intraoperative recordings, the stability in anesthetic level was assured by maintaining the bispectral index (BIS) at stable values in the range of 55–60 in all patients (Rosow and Manberg, 2001). No references to mesial recordings will be done in this work. The grid was placed over the lateral temporal cortex, with the border parallel to the Silvio fissure, and covering gyri T1–T3 (Fig. 1A) and, sometimes T4. The grid position was recorded either with a video camera or photographed. Reference electrode was at the nearby scalp, and in some cases was moved to the contralateral ear. Electrode grid orientation (parallel or perpendicular to the anterior–posterior temporal-lobe axis) varies from patient to patient due to surgical constraints (size of craniotomy, temporal lobe atrophy, localization of veins, etc.). Surgery was guided by raw ECoG data and other presurgical information, such as video EEG and MRI. Portions of the lateral temporal cortex, the amygdale and the hippocampus, were typically excised according to an anterior medial temporal resection (AMTR) tailored by ECoG (Spencer et al., 1984; Table 1). All of the analyses carried out in this paper were performed off-line. Thus, tailored lobectomy was not based on the results discussed here.

Intraoperative ECoG was recorded during 15–20 min using a 32-channel amplifier (Easy EEG II, Cadwell, USA), filtered at 0.5–400 Hz bandwidth. Data were exported to EDF format and then converted to ASCII (by using a SciLab script) for further off-line analysis. Artifact-free epochs lasting from 3 to 5 min were selected by visual inspection (Fig. 1B). By using consecutive, nonoverlapping windows of 1,024 data points (5.12 s at 200 Hz sampling rate) we obtain records of 16,384, 32,768 or 65,536 data points for each of the 20 channels. This time window allows encompassing most of the nonstationarities included

Table 1. Clinical and presurgical data

Patient	Age (years)	History of epilepsy (years)	Seizure type	MRI	v-EEG	Surgery	(one year)
1	34	22	Partial complex	Normal	L Mes	L AMTR	IIB
2	23	12	Partial complex	Lat R T tumor	R Lat	R AMTR	IA
3	48	13	Partial complex	R Hippo atrophy	L Mes	L AMTR	IIB
4	48	32	Partial complex	Bi-T MS (R > L)	Multifocalilty	R AMTR	IA
5	39	33	Partial complex	R MS and F-P atrophy	R Mes	L AMTR	IA
6	24	20	Partial complex	Normal	R Mes	R AMTR	IID
7	33	19	Partial complex	Normal	L Lat	L cortectomy	IIIA
8	27	23	Second. general	O Leucomalacia	L Mes	L AMTR	IIIA
9	39	3	Partial complex	Normal	R Lat	L AMTR	IA
10	44	29	Partial complex	Normal	L Mes	L AMTR	IA
11	42	9	Second. general	Unspecific L Mes. modification	R Mes	R AMTR	IA
12	44	27	Partial complex	Normal	L Mes	L AMTR	IA
13	32	31	Partial simple and complex	R MS	R Mes	R AMTR	IA
14	23	22	Partial complex	L MS	L Mes	L AMTR	ID
15	38	9	Partial simple and complex	Normal	L Mes	L AMTR	ID
16	46	43	Partial complex	Bi-T MS (L > R)	L Mes	L AMTR	IA
17	34	25	Partial complex	L pole tumor	L Mes	L cortectomy	IA
18	43	42	Second. general	R Hippo atrophy	L Mes	L AMTR	IA
19	24	23	Partial complex	Hemangioma R ventricle	R Mes	R AMTR	IA
20	59	35	Partial simple	R MS	R Mes	R AMTR	IA
21	48	32	Partial complex	R MS	R Mes	R AMTR	IIB
22	32	30	Partial complex	L MS	L Mes	L AMTR	IA
23	21	5	Partial complex	Normal	R Mes	R AMTR	IA
24	22	5	Partial complex	L MS	L Mes	L AMTR	IIIA
25	23	21	Partial complex	L MS	L Mes	L AMTR	IA
26	36	30	Second. general	Bi-F dysplasia	L Mes	L AMTR	IIB
27	41	38	Partial complex	L MS	L Mes	L AMTR	IA
28	55	42	Partial simple and complex	R MS	R Mes	R AMTR	IA
29	38	37	Partial simple and complex	L MS	L Mes	L AMTR	IA

Hippo, hippocampus; Bi, bilateral; Lat, lateral; Mes, mesial; MS, Mesial sclerosis; L, left; R, right; F, frontal; P, parietal; T, temporal; O, occipital; General, partial complex secondary generalized seizure; AMTR, anterior medial temporal resection.

in the time series. All analysis programs were written in GNU Fortran and running on a dual Opteron computer.

Synchronization analysis and spatial representation of intracortical interactions

Previous work has shown that there is not a clear a priori criterion for selecting a particular synchronization measure. Specifically, when dealing with neurophysiological data both linear and nonlinear types of measures seem to perform similarly (Quian Quiroga et al., 2002), whereas in some cases linear methods probed to be better (Netoff and Schiff, 2002). We therefore choose to apply a combination of linear and nonlinear synchronization measures to quantify the interdependence degree between cortical areas covered by the ECoG grid. To this purpose the Pearson correlation coefficient (*CO*), mutual information (*MI*), and phase synchronization (*PS*) were used. *CO* measures the linear cross-correlation between two ECoG time series. However, the absence of linear cross-correlation ($CO = 0$) does not exclude the presence of other kind of interactions, e.g., nonlinear correlations. In order to uncover more general correlations between two time series, *MI* and *PS* were introduced. *MI*, which is based in the concept of information, is directly related with the probability distributions p_i of the time series examined. *MI* quantifies how much extra information one gets from one time series by knowing the outcome of the other. If there is no relationship between the probability distributions of two time series, then $MI = 0$ and the two processes are independent. *MI* is a generalization of the *CO* measure since it is conceivable the case of two time series with $CO = 0$ and $MI > 0$, that is, linearly uncorrelated but statistically dependent. Finally, *PS*, which is also a nonlinear synchronization measure, is based in the concept of the instantaneous phase of a signal. *PS* is very useful for the analysis of chaotic and stochastic signals, for instance, which would be linearly uncorrelated but otherwise phase synchronized. As a first approximation, differences between *CO* against *PS* and *MI* would imply some kind of nonlinear coupling between two ECoG time series that are not adequately described solely by the *CO* measure. *CO*, *MI*, and *PS* are rigorously defined in the Appendix. In order to obtain normalized values for comparison, we estimated *PS* using the mean phase coherence (Mormann et al., 2000) and *MI* using the Granger statistic

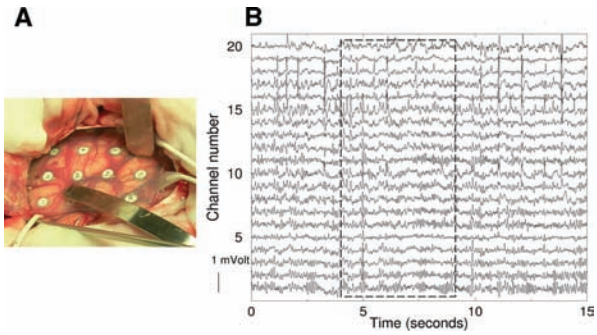

Figure 1.
(**A**) Representative view of the temporal lobe and the ECoG grid during the surgery, in this particular case from a right temporal epilepsy with the ECoG grid parallel to the antero (right)–posterior (left) axis. Up: superior; down: inferior. (**B**) Fifteen seconds of a representative ECoG recordings acquired using the 4 × 5 grid. The dashed line square represents the sliding temporal window used throughout the analysis.
Epilepsia © ILAE

(Granger and Lin, 1994). In this way, the three synchronization measures range from 0 (totally unsynchronized) to 1 (perfectly synchronized).

Synchronization measures were calculated by averaging in all the 5.2 s nonoverlapping moving windows (see above), for each pair of electrodes. Pairwise interactions between all 20 channels were represented in a matrix form (see Supplementary Fig. 1).

To facilitate visualization, results from the three synchronization matrices were represented spatially in the ECoG grid. To this purpose, for each channel we averaged interactions with its first neighbors to obtain a spatial map of the intracortical synchronization over the grid. The synchronization power of each channel of the grid is thus represented by intensity levels as

$$s_i = \frac{1}{n_i} \sum_{j=1}^{n_i} w_{ij} \qquad (1)$$

where w_{ij} is the synchronization value between electrodes i and j of the grid as obtained from either *CO*, *PS*, and *MI*. n_i is the number of first-neighbors in the i-electrode in the 4 × 5 grid. With this definition, local synchronization is restricted to cortical zones of radius < 1.42 cm (maximal interelctrode distance). This measure was previously introduced in the weighted network theory, although it is now normalized by its connectivity n_i (Barrat et al., 2004; Sporns et al., 2004). Therefore, the grid representation of intracortical interactions gives an idea on the contribution of each cortical area to synchronous activity, regardless whether it is located in the center ($n_i = 8$) or in a corner ($n_i = 3$) of the grid. We also located the maxima and minima of s_i values, $s_{\max}$and $s_{\min}$, and its channel positions, $i_{\max}$and $i_{\min}$, ($i = 1, 20$). Note that we will obtain different realizations of each value from each of the three corresponding methods, i.e., $i^{CO}_{\max}$, $i^{PS}_{\max}$, and $i^{MI}_{\max}$. A similar methodology aimed to uncover functional connectivity between brain areas has been used previously (Dodel et al., 2000; Eguíluz et al., 2005).

We also defined two measures to characterize the spatial features of the synchronization patterns. The grid intensity average $\bar{s}$ was defined as

$$\bar{s} = \frac{1}{20} \sum_{i=1}^{20} s_i \qquad (2)$$

with $s_i, i = 1, 20$. $\bar{s}$ represents a measure of the intensity distribution of the intracortical interactions. We also calculated the variance ($\bar{v}$) to quantify the overall deviation of the intensity values

$$\bar{v} = \frac{1}{20} \sum_{i=1}^{20} (s_i - \bar{s})^2 \qquad (3)$$

Surrogates

To statistically test synchronization patterns, we designed sets of surrogates of the original ECoG data (Prichard and Theiler, 1994; Pereda et al., 2005; Stam, 2005). We adopted a previously published approach to generate multivariate surrogate files by randomly time-shifting each of the 20 original time series (in the 4 × 5 grid) respect to each other and wrapping the extra values around to the beginning of the dataset (Netoff and Schiff, 2002). In this way, each channel in the surrogate file x_i^{surr}accounts for the same first-order statistical structure of the original, even though the temporal cross structure is destroyed. We generated 19 realizations for each of the 20 ECoG channels at each patient and data were reanalyzed to derive values of $\bar{s}$ and $\bar{v}$. The null hypothesis H_0 that there exist synchronization clusters of interictal activity in the lateral temporal cortex of TLE patients was tested using the z-score

$$Z = \frac{|<\theta^{surr}> - \theta\ |}{\sigma^{surr}} \qquad (6)$$

where θ is the value of $\bar{s}$ or $\bar{v}$ obtained from the original ECoG data and $<\theta^{surr}>$ is the mean value of $\bar{s}$ or $\bar{v}$ calculated from each of the 19 surrogate realizations. The null hypothesis can be rejected if $Z > 1.96$ at $p = 0.05$, which is equivalent to accept H_0 for the original data (Pereda et al., 2005).

ROC analysis

The Receiver Operating Characteristic analysis (ROC analysis) provides a tool to evaluate the result of predictions and has been extensively applied in medical research (Metz, 1978; Zweig and Campbell, 1993). It is particularly useful to define discrimination values for a binary classifier (true positive, true negative). We used ROC analysis to test the hypothesis that resection of synchronization

clusters at the lateral temporal cortex correlates with successful outcomes. Accordingly, the true positive category was defined as those cases where clusters were removed and good outcomes were reported, whereas the true negative was applied to the opposite. It is important to realize that our goal is to discriminate against a false positive that not removing synchronization clusters results in good outcomes. If the true positive case applies, ROC values are close to 1. ROC analysis was performed using MedCalc (http://www.medcalc.be/).

Results

Synchronization clusters in the lateral temporal cortex of TLE patients

Local interactions in the lateral temporal cortex in TLE were evaluated using three different synchronization measures, i.e., *CO*, *PS*, and *MI*. Synchronization matrices were obtained for each of the three methods using intraoperative ECoG data from 29 TLE patients (Supplementary Fig.1). To facilitate visualization, we plotted intracortical interactions over the grid by locally distributing synchronization values among channels according to Equation (1) for each of the three measures (Fig. 2A, B and C, upper row). Even though the total intensity is slightly different for each of the three synchronization measures, intensity distribution follows similar patterns. In the particular case shown in Fig. 2, higher levels of synchronization (yellow–orange) between channels 1, 2, 3, and 7 clearly depicted a cluster over the lateral temporal cortex. Lack of interactions was also detected (green–blue). See for instance, the lack of interactions of channel 20 with any other channel in the grid.

Surrogates of the original ECoG data confirmed that synchronization clusters were statistically significant. Shift surrogates were designed to preserve the statistical structure of the original ECoG data while destroying the correlations. Synchronization matrices obtained from surrogate datasets show this lack of interactions (Supplementary Fig.1). Grids obtained from the surrogate data clearly depicted the absence of synchronization (Fig. 2A, B and C, lower row). Therefore, clusters of synchronous interictal activity can be robustly defined in the lateral temporal cortex of TLE patients using a combination of synchronization methods and surrogate statistical analysis.

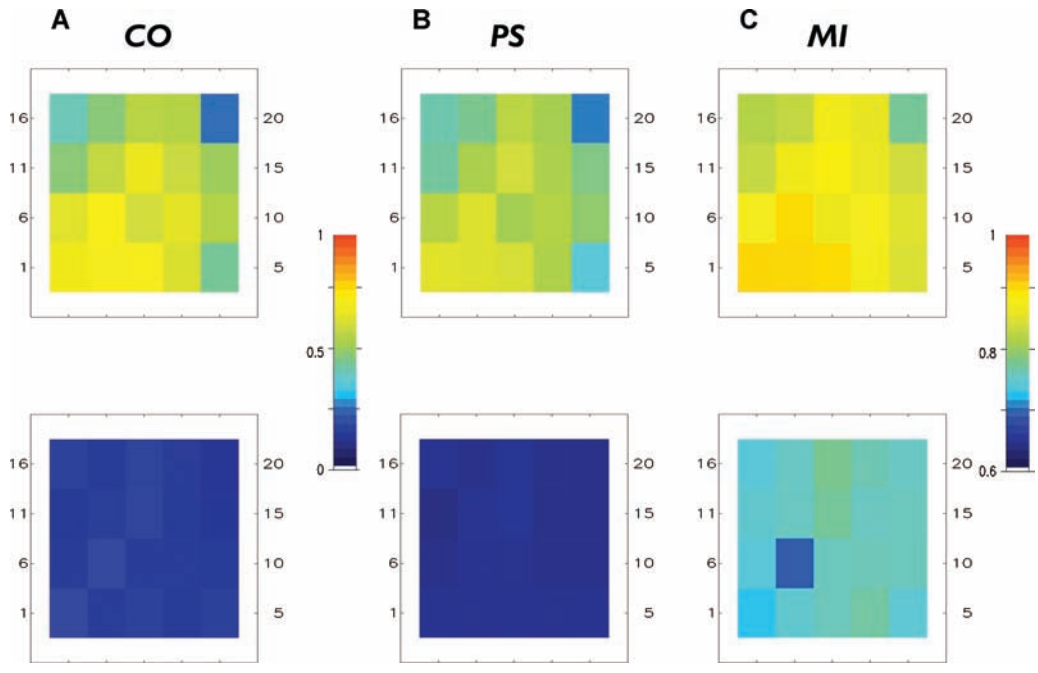

Figure 2.
(**A**) Grid representation (upper row) of intracortical interactions obtained from the cross-correlation (*CO*) analysis of the original ECoG data shown in Figure 1B and from one realization of surrogate data (lower row). (**B**) Same as in A for the phase synchronization (*PS*) analysis. (**C**) Same as in A for mutual information (*MI*). Note the difference in the scale between *CO* and *PS* and the one that correspond to *MI*. In the color-coded scale, blue (0 or 0.6) represents lack of synchronization and red (1) represents perfect synchronization.

MI performed worse than CO and PS for cluster detection

We characterized synchronization clusters mapped to the grid in terms of their mean intensity and variance ($\bar{s}$, $\bar{v}$). We calculated these parameters from the original and the surrogate ECoG data for each of the three methods (*CO*, *PS*, and *MI*). Supplementary Fig. 2 shows results obtained from the *CO* method but similar data were obtained for *PS* and *MI* (see Supplementary Figs. 3 and 4). In all three measures we found a large variability from patient to patient in the values of $\bar{s}$ and $\bar{v}$. Note for instance the case of patient #17, who showed a cluster of high intensity but lower $\bar{v}$, suggesting that synchrony was broadly distributed. In contrast, Patient 29 exhibited a cluster of averaged values of $\bar{s}$ but higher values of $\bar{v}$, suggesting that the synchronization cluster was sharply defined.

To test the values of $\bar{s}$ and $\bar{v}$ we used surrogated datasets. We quantified statistically the difference between the values of $\bar{s}$ and $\bar{v}$ in the original and the surrogated ECoG data using the z-score with the discrimination threshold at $z > 1.96$ ($p = 0.05$). Supplementary Fig. 5 shows z-scores for each of the three methods; *CO* (solid circles), *MI* (empty squares), and *PS* (solid diamonds). We found that $\bar{s}$ values obtained from the three methods were statistically significant (Supplementary Fig. 5, left). However, this was not true for $\bar{v}$ values that performed poorly when compared with surrogates (Supplementary Fig. 5, right). This was particularly clear for *MI*, which yielded values of $\bar{v}$ below the corresponding threshold in 8 of 29 patients. The other two methods, *CO* and *PS*, performed better with the only exception of Patient 1. This poor performance of *MI* can be related with data length problems. A robust estimation of the bidimensional probability distribution needed for calculating *MI* requires much more data that was actually done in our calculations (Quian Quiroga et al., 2002), which is severely constrained by the total length of the intraoperative ECoG data files. Longer temporal windows would improve *MI* estimation in each window, but would decrease the final averaged value.

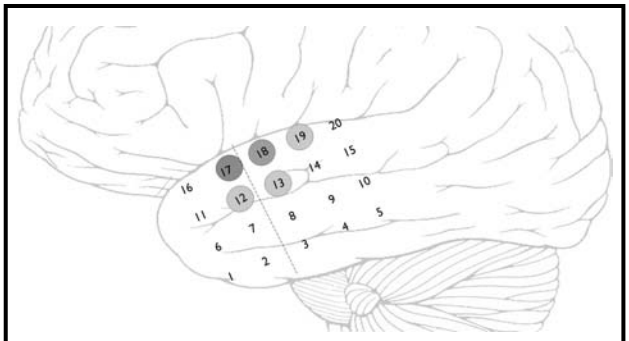

Figure 4.
Schematic representation of the spatial relationship between synchronization clusters and surgery. A grid of electrodes (1 to 20) is represented in the temporal lobe and the resected area is marked by a dashed line. Intensity levels of intracortical interactions are color-coded in a gray scale. Electrode number 17 corresponds to the cluster maxima followed in intensity by electrodes 18, 12, 13, and 19. When clusters are defined using the three most intense electrodes (here, electrodes 17, 18, and 12), surgery has removed 66% of the cluster (electrodes 17 and 12). If all the five most intense electrodes are considered, then only 40% of the cluster has been removed.
Epilepsia © ILAE

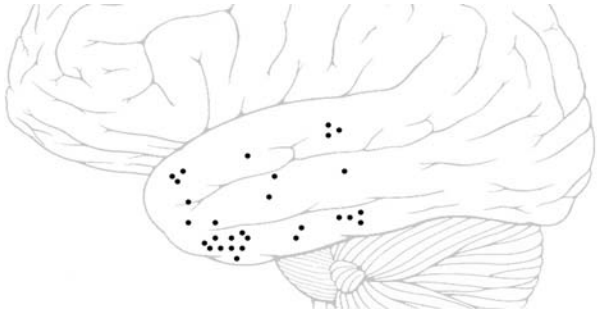

Figure 3.
Cluster's maxima (*CO*) localization over the lateral temporal cortex. The position of cluster's maxima for each patient (Table 2) is roughly represented over the lateral temporal lobe according to anatomical information recorded intraoperatively (grid position, photographs, videos, and drawing notes). Clusters maxima were scattered all over the temporal lobe at T1 (29% patients), T2 (20%), and T3 (51%), with propensity to distribute at the anterior (55%) than at the mid (17%) and posterior (28%) temporal lobe.
Epilepsia © ILAE

Spatial features of synchronization clusters

We then examined the spatial features of synchronization clusters by calculating the position (i_{max}) of the maximum intensity obtained from each of the three methods. Results are summarized in Table 2. Clusters maxima were scattered all over the temporal lobe and typically involved up to four or five electrodes ($\sim$ 4-5 cm long). We evaluated whether clusters were typically related with sulcus or gyral boundaries. To this purpose we looked at the location of the first and second cluster maxima (*CO*) in each patient. We found that in 15 patients both maxima were located at the same gyrus, whereas 14 patients exhibited clusters covering two adjacent gyri; i.e., there was a sulcus in between. As illustrated in Table 2 and Fig. 3,

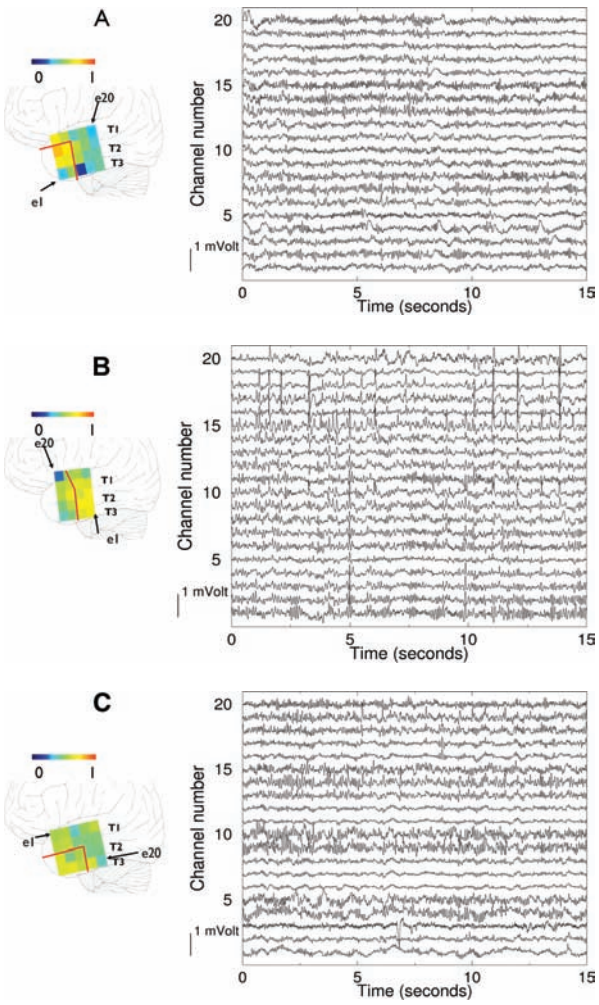

Figure 5.
Synchronization clusters and surgical outcome. Solid red lines indicate the cortical area removed during the surgery. Grid representation of intracortical interactions (left panel) and a short epoch of the corresponding raw data (right panel) are also depicted. e1 and e20 stands for electrode 1 and electrode 20, respectively. In the color-coded scale, blue (0) represents lack of synchronization and red (1) represents perfect synchronization. (A) Patient 2 exhibited a sharply defined cluster ($\bar{v}$= 0.026) and surgery outcome was IA (no crisis). Here the surgical procedure resulted in removing most of the synchronization cluster. (B) Patient 21 is a representative example of sharply defined clusters ($\bar{v}$= 0.013) that were not surgically removed. Surgery outcome was IIB. (C) Patient 8, who showed no clear boundaries of synchronization cluster, had a $\bar{v}$= 0.0053. Despite surgery in this case has removed part of the cluster, some regions of higher intracortical synchronization has been spared. Surgical outcome was IIIA.

clusters maxima were found at T1 (29% patients), T2 (20%), and T3 (51%), with larger propensity to distribute at the anterior (55%) than at the mid (17%) and posterior (28%) temporal lobe. Therefore, cluster maxima can be detected all over the temporal lobe, with a predisposition to be located at the anterior T3 gyrus (35%).

Regarding colocalization of cluster maxima by different synchronization methods, we found that in 83% of the sample (24 patients), the location of the cluster maximum defined from *CO* and *PS* coincided, i.e., $i_{\max}^{CO} = i_{\max}^{PS}$. Because of the coarse spatial resolution of the electrode grid, we considered as "coincidences" those cases where maxima laid in adjacent positions. In all these cases the position of the cluster maximum calculated from *MI* ($i_{\max}^{MI}$) coincided with that detected by *CO* and *PS*; that is $i_{\max}^{CO} = i_{\max}^{PS} = i_{\max}^{MI}$ (Table 2). In three of the remaining five patients, *CO* and

Table 2. Coincidence of synchronization clusters' maxima defined from *CO*, *PS*, and *MI*

Patient	Engel	Detection method CO	PS	MI	Position in temporal lobe	$\bar{v}$ ($\times 10^2$)
$i_{\max}^{CO} = i_{\max}^{PS} = i_{\max}^{MI}$(a)						
2	IA	11	11	11	T1/T2 A	2.6656
3	IIB	19	19	19	T3 A	1.6383
4	IA	2	2	2	T3 A	2.6200
5	IA	3	3	3	T1 M	1.5538
6	IID	8	8	8	T2 M	1.0722
7	IIIA	16	16	16	T3 A	0.5789
8	IIIA	17	17	17	T3 A	0.5330
11	IA	18	18	18	T3 M	0.9166
12	IA	3	3	7	T1/T2 M	0.9800
13	IA	16	16	16	T1 A	0.6699
14	ID	11	11	11	T2/T3 A	0.5150
15	ID	6	6	6	T1 A	2.9277
16	IA	5	5	5	T1 P	2.2608
17	IA	16	16	16	T3 A	0.5269
18	IA	7	7	7	T2 A	1.4132
19	IA	1	1	1	T3 A	1.7552
21	IIB	7	1	2	T3 P	1.3377
22	IA	16	16	16	T3 A	1.3971
23	IA	2	2	2	T3 A	1.7909
24	IIIA	14	13	18	T1 P	2.5230
26	IIB	17	17	17	T3 P	3.0876
27	IA	5	5	5	T3 A	1.3913
28	IA	16	16	16	T3 P	0.9562
29	IA	13	13	18	T2 P	3.8819
$i_{\max}^{CO} = i_{\max}^{PS} \neq i_{\max}^{MI}$ (a)						
1	IIB	19	19	6	T3 P	0.2239
10	IA	11	11	5	T3 A	0.6810
20	IA	4	3	11	T3 M	0.7267
$i_{\max}^{CO} \neq i_{\max}^{PS} \neq i_{\max}^{MI}$(a)						
9	IA	19	7	5	T1 P	0.6953
25	IA	20	2	6	T1 A	0.8373

A, Anterior; M, Middle; P, Posterior.
(a) Coincidence includes the case of adjacent electrodes.

Table 3. ROC analysis

	Entire group			First 15 patients ([a])			Last 15 patients ([b])		
	Area	SE	p	Area	SE	p	Area	SE	p
Highest maxima	0.616	0.111	0.150	0.527	0.154	0.431	0.900	0.083	<0.0001
Two highest maxima	0.639	0.110	0.103	0.580	0.152	0.299	0.900	0.083	<0.0001
Three highest maxima	0.658	0.108	0.071	0.634	0.149	0.184	0.910	0.075	<0.0001
Four highest maxima	0.668	0.104	0.05	0.607	0.150	0.238	0.900	0.081	<0.0001
Five highest maxima	0.718	0.096	0.01	0.634	0.147	0.182	0.890	0.088	<0.0001

([a]) lower $\bar{v}$; ([b]) higher $\bar{v}$

Area under the ROC curve (area), standard error (SE), and p-value (P) in each of the three groups (see text). Patient list has been ordered (ascending) accordingly with correlation variance. The first 15 patients had broadly distributed intracortical interactions and the last 15 patients show sharply defined synchronization clusters.

PS maxima were located at the same electrode, but *MI* did not colocalized, i.e., $i_{\max}^{CO} = i_{\max}^{PS} \neq i_{\max}^{MI}$. In the remaining two cases no coincidence were detected with any method, i.e., $i_{\max}^{CO} \neq i_{\max}^{PS} \neq i_{\max}^{MI}$ (Table 2). The poor performance of *MI* for cluster discrimination appeared to account for this discrepancy. However, we also noted that in the five cases where maxima did not match, synchronization clusters typically showed low $\bar{v}$ values (Table 2), suggesting that colocalization fails when synchrony is broadly distributed.

Sharply defined synchronization clusters and surgical outcomes

Are synchronization clusters relevant to TLE? We addressed this question by examining the effect of removing synchronization clusters in surgery outcome. Most patients included in this analysis exhibited Engel classes I and II after a year follow-up, with only three cases of Engel's class III (Engel et al., 1993). Because we wanted to highlight subtle differences in patient-to-patient variability, surgical outcomes were evaluated using the detailed Engel's scheme (Engel et al., 1993). According to this classification an Engel IA corresponds to completely seizure free, whereas other classifications state for different frequency of seizures. We found that 19 patients (65%) exhibited an Engel IA whereas the remaining 10 patients experience some kind of seizures after the surgery (two patients with ID; four patients with IIB, one patient with IID, and three patients with IIIA; see Table 2).

We performed ROC analysis to test the hypothesis that resection of synchronization clusters correlates with an Engel IA outcome (true positive). To define the limits of synchronization clusters, we used the location of the cluster maxima and up to its five more intense neighbors to examine the spatial relationship between clusters and surgery. Data were organized according to the percentage of the cluster that was surgically removed (Fig. 4). Because of the location of cluster maxima calculated from *CO* and *PS* did not differ in most of the sample, we choose to use clusters defined from *CO* analysis. The two cases where $i_{\max}^{CO} \neq i_{\max}^{PS}$ were analyzed independently. Results are summarized in Table 3 (see the entire group column). We found no strong evidence that a complete resection of synchronization clusters would result in a good surgical outcome.

However, large patient-to-patient variability in the definition of clusters might obscure clinical correlations. We therefore ordered data according to its $\bar{v}$ values, with large $\bar{v}$ meaning sharpest clusters, and low $\bar{v}$ values meaning a broader synchronization distribution. ROC analysis was performed for the top 15 patients exhibiting blurred clusters (lower $\bar{v}$ values) and for the bottom 15 patients with sharp clusters (large $\bar{v}$). We found that ROC results for the first 15 patients were poor; suggesting that broadly distributed synchronization is not related with surgical outcome. However, the ROC curve for the last 15 patients is equal or even greater than 0.89 and in all cases with a p-value lower than 0.0001.

Fig. 5 shows three representative examples of the above results. Patients in Fig. 5A and B exhibited sharply delimited clusters over the lateral temporal cortex. In the first case (Fig. 5A), most of the synchronization cluster was surgically removed and surgical outcome was Engel IA. In the second case (Fig. 5B), most of the sharply delimited synchronization cluster was not removed and surgical outcome was poor (Engel IIB). A typical case of broadly distributed synchronization clusters is depicted in Fig. 5C. Here, in spite of a nearly complete removal of synchronization maxima, surgical outcome was poor (Engel IIB). Overall, our results indicate that when synchronization clusters are sharply detected, surgical removal will correlate with better seizure control, no matter whether clusters were located at the anterior or the posterior temporal lobe.

Raw data are also included in Fig. 5 for comparison. Although a one-to-one visual connection between ECoG raw data and synchrony representation in the grid is not always straightforward (e.g., Fig. 5A), mainly due to the additive process in Equation (1), some relationships between synchronization and ECoG activity can be easily seen. See for example Fig. 5B, which clearly shows strong synchronization between channels 1, 2, 3, 6, and 7. Channels 5, 16, and, mostly, channel 20 seem to move independently from

its neighbors. Fig. 5C shows a case of more widespread synchronization. Channels 2, 6, 7, 8, 16, 17, and 18 are to a certain extent synchronized. Note that ECoG raw data from channel 8 are highly synchronous with channel 7, but its deficient synchronization with neighboring channels 9, 12, and 13 results in a low synchronization map in the grid representation. This fact helps to further understand the meaning of the grid representation. Higher values of s_i symbolize high synchronization between channel e_i and most of its neighbors, as is the case of channel 2 in Fig. 5B.

As a last point it is interesting to note that out of the eight patients with cluster maxima located at the posterior part of the temporal lobe (see Table 2 and Supplementary Fig. 4), four of them suffered further seizures after the surgery (three IIB and 1 IIIA). In all of these four cases, cluster maxima have not been removed. This fact is independent of whether the synchronization cluster was broadly distributed (Patients 1 and 28) or sharply defined (patients #21 and #24). On the other side, the sharpest defined cluster in the sample, that is, Patient 29 with its maxima located at the posterior part of T2 results in an Engel IA with its maxima been removed during the surgery. This point is important because quite generally the posterior part of the temporal lobe is not removed in an AMTR.

Discussion

Our results show that intracortical interactions are distributed inhomogeneously over the lateral temporal cortex of TLE patients. In particular, synchronization clusters of ECoG activity can be characterized using different quantitative measures such as cross-correlation, mutual information, and phase synchronization. Our findings suggest that synchronous ECoG activity emerges from specific cortical sites that in some cases are highly differentiated from the rest of the temporal cortex. Although there exists several degrees of intensities, ranging from sharp peaks to almost evenly distributed interactions, clusters are clearly detected in most cases. ROC analysis shows that surgical removal of sharply defined synchronization clusters correlated with seizure control, suggesting that these sites might be involved in the circuits that participate in seizure generation.

The existence of cortical regions exhibiting higher levels of synchronization during ECoG activity has been previously suggested. Towle and coworkers reported a local increase of coherence during the interictal period and linked this information with the underlying architecture of the epileptic temporal lobe (Towle et al., 1998, 1999). Using different synchronization measures (*CO*, *PS*, and *MI* included) other groups have provided evidence that the seizure onset zone exhibits higher synchronization than any other region (Arnhold et al., 1999; Mormann et al., 2000; Bartolomei et al., 2004). Indeed, there are reports of increased levels of several synchronization measures during the interictal period in the focal hemisphere compared with the contralateral pole, as measured by EEG analysis (Kraskov, 2004). It might be possible that synchronization clusters detected intraoperatively in the targeted temporal lobe might be the substrate for increased levels of synchronization in this region.

Here, we applied three general synchronization measures to evaluate the pattern of interactions recorded in the lateral temporal cortex of TLE patients during surgery. Although from a methodological point of view, *CO* and *PS* appear to be statistically more robust than *MI*, the three methods localize cluster maxima at the same position in most cases, which would imply the existence of linear coupling among different cortical sites. Synchronization clusters were not homogeneous between different patients, neither was their definition over the lateral temporal cortex. It is possible that the inhomogeneous nature of synchronization clusters can be linked to specific alterations of the underlying neuronal circuits in TLE. In spite of the clear columnar organization of the cerebral cortex, widespread horizontal excitatory connections provide pathways for the propagation of interictal and ictal activity (Shepherd, 1997; Chervin et al., 1988). Local intracortical interactions are under the influence of local inhibitory circuits that act to control runway excitation (Shepherd, 1997; Connors, 1997). Immunohistochemical, genetic, and electrophysiological studies have provided evidence of an abnormal patchy organization of the inhibitory circuits of the lateral temporal cortex of TLE patients (Ferrer et al., 1994; Marco et al., 1996; Menendez de la Prida et al., 2002; Arion et al., 2006). It has been also demonstrated that a local decrease of GABAergic terminals correlates with increased expression of different glutamatergic receptors such as GluR2/3 and GluR5 (DeFelipe et al., 1994; Gonzalez-Albo et al., 2001). These inhomogeneities in the excitatory and inhibitory balance over the lateral temporal cortex could be the cellular basis for increased levels of synchronization detected as spatially segregated clusters.

Are these clusters relevant to TLE surgery? We found that when synchronization clusters are sharply defined, as detected by elevated values of $\bar{v}$, removal of this area, or a great part of it, statistically correlates with seizure control. This suggests that these sites might be connected to the circuits that participate in seizures. Regions involved in clinical seizures in TLE are diverse and widespread. A definition of up to six areas relevant for the generation of interictal and ictal activity clearly demonstrate that not a single region is involved but interaction among them is crucial (Rosenow and Luders, 2001; Bartolomei et al., 2005; Pastor et al., 2006). Synchronization clusters of intraoperative ECoG activity are detected over the lateral temporal cortex and their definition vary from patient to patient. These suggest that they are not likely to result from intrinsic connectivity; instead they might be the expression of altered circuitry in the temporal lobe of TLE patients. Very recently, Garcia Dominguez et al. (2005) showed that

clinical seizures proceed by the recruitment of neighboring, i.e., local, neuronal networks separated less than 4 cm. This is in accordance with the spatial scale of synchronization clusters we found in our study (i.e., 4-5 cm). Although there is report of fluctuating levels of synchrony between different cortical areas during the interictal, preictal and the ictal periods (Mormann et al., 2003; Bartolomei et al., 2005), previous data suggest that synchronized activity may be a feature of the seizure onset zone (Arnhold et al., 1999; Morman et al., 2000; Garcia-Dominguez et al., 2005). Synchronization clusters may thus provide a gate for activity to spread within the temporal lobe, which may explain why in those cases where sharply defined cluster were not excised seizures continue to occur. We also observed no correlation with surgical outcomes if broadly distributed clusters were detected. In these cases removing these regions did not appear to improve outcomes. One possibility is that a poor definition of synchronization clusters might reflect the absence of structural alterations of the underlying circuits. Another alternative is that the synchronization region over the lateral temporal lobe was not sampled by the electrode grid and therefore there is no information on a relationship with surgery. Future work aimed to explore the functional dynamics of synchronous cortical activity over the entire temporal lobe would be essential to understand the exact topography of the several areas underlying seizure generation. In particular, it might be important to address questions on the relationship between synchronization clusters and seizure onset and propagation.

Acknowledgments

We thank Dr. S.S. Spencer for helpful comments on the elaboration of this manuscript. This work has been funded by grants from the Ministerio de Sanidad FIS CP04/00216, UBACyT X074, PIP CONICET 5164 (GJO) and from the Instituto de Salud Carlos III PI060349 (JP,RGS,GJO). GJO is also a member of the Consejo Nacional de Investigaciones Científicas y Técnicas (CONICET), Argentina.

References

Arion D, Sabatini M, Unger T, Pastor J, Alonso-Nanclares L, Ballesteros-Yanez I, Garcia Sola R, Munoz A, Mirnics K, DeFelipe J. (2006) Correlation of transcriptome profile with electrical activity in temporal lobe epilepsy. *Neurobiol Dis* 22(2):374–387.

Arnhold J, Lehnertz K, Grassberger P, Elger CE. (1999) A robust method for detecting interdependences: application to intracranially recorded EEG. *Physica D* 134:419–430.

Barrat M, Barthelemy R, Pastor-Satorras, Espignani A. (2004) The architecture of complex weighted networks. *Proc Natl Acad Sci USA* 101:3747.

Bartolomei F, Wendling F, Regis J, Gavaret M, Guye M, Chauvel P. (2004) Pre-ictal synchronicity in limbic networks of mesial temporal lobe epilepsy. *Epilepsy Res* 61:89–104.

Chervin RD, Pierce PA, Connors BW. (1988) Periodicity and directionality in the propagation of epileptiform discharges across neocortex. *J Neurophysiol* 60:1695–1713.

Connors BW. (1997) Neocortical anatomy and physiology. In Jerome E. Jr, Timothy A (Eds) *Epilepsy a comprehensive textbook. Vol 1* Pedley, Lippincot-Raven, New York, pp. 307–322

DeFelipe J, Huntley GW, del Rio MR, Sola RG, Morrison JH. (1994) Microzonal decreases in the immunostaining for non-NMDA ionotropic excitatory amino acid receptor subunits GluR 2/3 and GluR 5/6/7 in the human epileptogenic neocortex. *Brain Res* 657(1–2):150–158.

Dichter MA, Ayala GF. (1987) Cellular mechanism of epilepsy: a status report. *Science* 237:157–164.

Dodel S, Herrmann JM, Geisel T. (2000) Localization of brain activity—blind separation for fMRI data. *Neurocomputing* 701:32–33.

Dümpelmann M, Elger CE. (1999) Visual and automatic investigation of epileptiform spikes in intracranial EEG recordings. *Epilepsia* 40:275–285.

Eguiluz VM, Chialvo DR, Cecchi GA, Baliki M, Apkarian V. (2005) Scale-free brain functional networks. *Phys Rev Lett* 94:018102.

Engel, J Jr., Van Ness PC, Rasmussen TB, Ojemann LM. (1993) Outcome with respect to epileptic seizures. In Engel J Jr. (Ed) *Surgical treatment of the epilepsies*. Raven Press, New York, p. 609

Ferrer I, Oliver B, Russi A, Casas R, Rivera R. (1994) Parvalbumin and calbindin-D28k immunocytochemistry in human neocortical epileptic foci. *J Neurol Sci* 123:18–25.

Garcia Domínguez L, Wennberg RA, Gaetz W, Cheyne D, Snead OC III, Perez Velazquez JL. (2005) Enhanced synchrony in epileptiform activity? Local versus distant phase synchronization in generalized seizures. *J Neurosci* 25(35):8077–8084.

Gonzalez-Albo MC, Gomez-Utrero E, Sanchez A, Sola RG, DeFelipe J. (2001) Changes in the colocalization of glutamate ionotropic receptor subunits in the human epileptic temporal lobe cortex. *Exp Brain Res* 138(3):398–402.

Granger C, Lin J. (1994) Using mutual information coefficient to identify lags in nonlinear models. *J Time Series Anal* 15(4):371–384.

Gray CM, König P, Engel AK, Singer W. (1989) Oscillatory responses in cat visual cortex exhibit inter-columnar synchronization which reflects global stimulus properties. *Nature* 338:334–337.

Keene DL, Whiting S, Ventreyra EC. (2000) Electrocorticography. *Epileptic Disord* 2:57–63.

Kraskov A. (2004) Applications of synchronization and interdependence measures in particular to EEG of epilepsy patients. PhD thesis John Von Neumann Institute for computing, NIC series Vol. 24.

Lüders, HO. (1992) *Epilepsy surgery*. Raven Press, New York.

Marco P, Sola RG, Pulido P, Alijarde MT, Sanchez A, Ramon y Cajal S, DeFelipe J. (1996) Inhibitory neurons in the human epileptogenic temporal neocortex. An immunocytochemical study. *Brain* 119:1327–1347.

McKhann GM, Schoenfeld-McNeill J, Born DE, Haglund MM, Ojemann GA. (2000) Intraoperative hippocampal electrocorticography to predict the extent of hippocampal resection in temporal lobe epilepsy surgery. *J Neurosurg* 93:44–52.

Menendez de la Prida L, Benavides-Piccione R, Sola R, Pozo MA. (2002) Electrophysiological properties of interneurons from intraoperative spiking areas of epileptic human temporal neocortex. *Neuroreport* 13:1421–1425.

Metz CE. (1978) Basic principles of ROC analysis. *Seminars Nucl Med* VIII:283–298.

Mormann F, Kreuz T, Andrzejak RG, David P, Lehnertz K, Elger CE. (2003) Epileptic seizures are preceded by a decrease in synchronization. *Epilepsy Res* 53:173–185.

Mormann F, Lehnertz K, David P, Elger CE. (2000) Mean phase coherence as a measure for phase synchronization and its application to the EEG of epilepsy patients. *Physica D* 144:358–369.

Netoff TI, Schiff SJ. (2002) Decreased neuronal synchronization during experimental seizures. *J Neurosci* 22:7297–7307.

Nunez P. (1993) *Electric fields in the brain*. Cambridge University Press, Cambridge.

Pastor J, Hernando V, Domínguez-Gadea L, De Llano I, Meilán ML, Martínez-Chacón JL, Sola RG. (2005) Impact of experience on improving the surgical outcome in temporal lobe epilepsy. *Rev Neurol* 41:709–716.

Pastor J, Menéndez dela Prida L, Hernando V, Sola RG. (2006) Voltage sources in mesial temporal lobe epilepsy recorded with foramen ovale electrodes. *Clin Neurophysiol* 117(12):2604–2614.

Pereda E, Quian Quiroga R, Bhattacharya J. (2005) Nonlinear multivariate analysis of neurophysiological signal. *Progress Neurobiol* 77:1–37.

Pikovsky AS, Rosenblum MG, Osipov GV, Kurths J. (1997) Phase synchronization of chaotic oscillators by external driving. *Physica D* 79:219.

Prichard D, Theiler J. (1994) Generating surrogate data for the time series with several simultaneously measured variables. *Phys Rev Lett* 73: 951–955.

Quian Quiroga R, Kraskov A, Kreuz T, Grassberger G. (2002) Performance of different synchronization measures in real data: a case study on electroencephalographic signals. *Phys Rev E* 65:041903.

Rosenblum MG, Pikovsky AS, Kurths J. (1996) Phase synchronization of chaotic oscillators. *Phys Rev Lett* 76:1804–1807.

Rosenblum MG, Pikovsky AS, Kurths J, Schaefer C, Tass P. (2001) Phase synchronization: from theory to data analysis. In Moss F, Gielen S (Eds) *Handbook of biological physics*, Elsevier Science, Amsterdam, 2001, p. 297.

Rosenow F, Lüders HO. (2001) Presurgical evaluation of epilepsy. *Brain* 124:1683–1700.

Rosow C, Manberg PJ. (2001) Bispectral index monitoring. *Anesthesiol Clin North America* 19:947–966.

Shepherd GM. (1997) *The synaptic organization of the brain*. 4th Ed. Oxford University Press, New York.

Schwartz TH, Bazil CW, Walczak TS, Chan S, Pedley TA, Goodman RR. (1997) The predictive value of intraoperative electrocorticography in resections for limbic epilepsy associated with mesial temporal sclerosis. *Neurosurgery* 40:302–309.

Sola RG, Hernando V, Pastor F, Navarrete EG, Felipe J, Alijarde MT, Sánchez A, Domínguez L, Martín P, Maestú F, de Felipe-Oroquieta J, Ramón y Cajal S, Pulido P. (2005) Pharmacoresistant temporal-lobe epilepsy. Exploration with foramen ovale electrodes and surgical outcomes. *Rev Neurol* 41:4–16.

Spencer DD, Spencer SS, Mattson RH, Williamson PD, Novelly RA. (1984) Access to the posterior medial temporal lobe structures in the surgical treatment of temporal lobe epilepsy. *Neurosurgery* 15:667–671.

Sporns O, Chialvo DR, Kaiser M, Hilgetag CC. (2004) Organization, development and function of complex brain networks. *Trends Cogn Sci* 8:418–425.

Stam CJ. (2005) Nonlinear dynamical analysis of EEG and MEG: review of an emerging field. *Clin Neurophysiol* 116:2266–2301.

Towle VL, Syed I, Berger C, Grzesczuk R, Milton J, Ericsson RK, Cogen P, Berkson E, Spire JP. (1998) Identification of the sensory/motor area and pathologic regions using ECoG coherence. *Electroencephalogr Clin Neurophysiol* 106:30–39.

Towle VL, Carder RK, Khorasani L, Lindberg D. (1999) Electrocorticographic coherence patterns. *J Clin Neurophysiol* 16:528–547.

Wilson SB, Emerson R. (2002) Spike detection: a review and comparison of algorithms. *Clin Neurophysiol* 113:1873–1881.

Zweig MH, Cambell G. (1993) Receiver-operating characteristic (ROC) plots: a fundamental evaluation tool in clinical medicine. *Clin Chem* 39:551–577.

APPENDIX

Each ECoG record **x**is a multivariate dataset of N_{chan} channels, 20, and N_{dat}data points, 16,384, 32,768 or 65,536 in each channel

$$\mathbf{x} = x_i(k), i = 1, N_{chan} \quad \text{and} \quad k = 1, N_{dat}$$

where subindex i represent the channel number and k is the discretized time. In our calculations we have sectioned the analysis in windows of nonoverlapping N_{win}= 1,024 data points.

Linear correlation analysis (CO)

Linear CO was performed by using the traditional correlation coefficient estimated between two time series, which at lag = 0 is nothing else but the Pearson's coefficient. In our case, ρ_{ij}represent the cross-correlation between channels i and j

$$\rho_{ij}(0) = \frac{\sum_{k=1}^{N_{win}} (x_i(k) - \overline{x_i})(x_j(k) - \overline{x_j})}{\sqrt{\sum_{k=1}^{N_{win}} (x_i(k) - \overline{x_i})^2 \sum_{k=1}^{N_{win}} (x_j(k) - \overline{x_j})^2}} \quad \text{(A1)}$$

Because $-1 \leq \rho_{ij} \leq 1$, we have used the absolute value of ρ_{ij}, that is $|\rho_{ij}|$. This is so because we are interested in the linear correlation regardless if it is direct or inverse, and in this way naming $Co_{ij} = |\rho_{ij}|$ we have:

$$0 \leq Co_{ij} \leq 1 \quad \text{(A2)}$$

Calculations done with Co_{ij}between the two channels i and j will be called generically CO.

Phase synchronization (PS)

The concept of phase synchronization, introduced by Rosenblum et al. (Rosenblum et al., 1996) in relation to chaotic oscillators has been increasingly used in the last years, especially in the field of neuroscience (Rosenblum et al., 2001; Garcia Dominguez et al., 2005). It has been also extended to the case of noisy oscillators (Pikovsky et al., 1997). The power of the method resides in that it measures the phase relationship, independently on the signal amplitude. In order to evaluate differences between phases in two signals, one must firstly define the instantaneous phase of the signal, by means of the analytical signal concept. For a continuous signal $x_i(t)$ the associated analytical or complex signal is defined as

$$z_i(t) = x_i(t) + i\tilde{x}_i(t) = A_i(t)e^{i\phi_i(t)}$$

where $\tilde{x}_i(t)$is the Hilbert transform of $x_i(t)$

$$\tilde{x}_i(t) = \frac{1}{\pi} p.v. \int_{-\infty}^{\infty} \frac{x(t')}{t - t'} dt' \quad \text{(A3)}$$

where $p.v.$ stands for (Cauchy) Principal Value. The instantaneous phase is thus,

$$\phi_i(t) = \arctan \frac{\tilde{x}_i(t)}{x_i(t)} \quad \text{(A4)}$$

And the phase difference between the two signals can be calculated as

$$\phi_i(t) - \phi_j(t) = \arctan \frac{\tilde{x}_i(t)x_j(t) - x_i(t)\tilde{x}_j(t)}{\tilde{x}_i(t)x_j(t) + x_i(t)\tilde{x}_j(t)} \quad \text{(A5)}$$

In order to implement numerically the above definition over two time series $x_i(k)$ and $x_j(k)$, the mean phase coherence (R_{ij}) was introduced (Mormann et al., 2000)

$$R_{ij} = \left| \frac{1}{N_{win}} \sum_{k=1}^{N_{win}} e^{i\Delta\alpha_{ij}(k)} \right| \quad \text{(A6)}$$

calculated in the time window N_{win}, where $\Delta\alpha_{ij}(k) = \phi_i(k) - \phi_j(k)$ is the instantaneous phase difference at the discretized time k. It is clear from Equation (A6) that R_{ij} follows the same relation as Equation (A2), that is $0 \leq R_{ij} \leq 1$. The literature (Rosenblum et al., 2001) gives useful hints for the numerical calculation of the Hilbert Transform of a time series, i.e., Equation (A3). Calculations done with R_{ij} between the two channels i and j will be called generically *PS*.

Mutual information (MI)

For a single time series, x_i of length N_{win} one can estimate its probability distribution, $P(x_i)$ by partitioning the entire range of values taken by x_i in N_{bins} bins and then, count the number of points n_l falling in each bin l. In this way, the relative occurrence n_l/N_{win} estimates $p_i(l)$, the probability that a point in the time series i fall in the bin l. Then, the Shannon entropy is defined as

$$H\left[P(x_i)\right] = H(x_i) = -\sum_{l=1}^{N_{bins}} p_i(l)\log_2 p_i(l)$$

for time series x_i, and likewise

$$H\left[P(x_j)\right] = H(x_j) = -\sum_{l=1}^{N_{bins}} p_j(l)\log_2 p_j(l)$$

for time series x_j

Analogously, using the joint probability distribution $P(x_i, x_j)$, the joint entropy between x_i and x_j (or properly between $P(x_i)$ and $P(x_j)$) is

$$H[P(x_i, x_j] = H(x_i, x_j) = -\sum_{l=1}^{N_{bins}}\sum_{k=1}^{N_{bins}} p_{ij}(l,k)\log_2 p_{ij}(l,k)$$

Finally, the mutual information $MI(x_i, x_j)$ between x_i and x_j is

$$MI(x_i, x_j) = H(x_i) + H(x_j) - H(x_i, x_j)$$

which clearly shows that it is a symmetric function of x_i and x_j. *MI* is positive, being zero when the probabilities distributions of x_i and x_j are independent. *MI* can be thought as a generalization of the linear correlation coefficient. It gives the reduction in the uncertainty in x_i due to the knowledge of x_j. We have estimate *MI* using the above procedure, using bins of size 30 through 50 with similar results. All the results present in this paper correspond to $N_{bins} = 30$.

Although *MI* is bounded from below, giving $MI = 0$ when there is statistical independence between x_i and x_j, it is not bounded from above. In this context it is useful to define a mutual information statistic (Granger and Lin, 1994) with the property of Equation (A2),

$$\lambda_{ij} = \sqrt{1 - e^{-2MI_{ij}}}$$

which now satisfies $0 \leq \lambda_{ij} \leq 1$. Calculations done with λ_{ij} between the two channels i and j will be called generically *MI*.

Supplementary Material

The following supplementary material is available for this article:

Supplementary Figure 1: Synchronization matrices. Upper row shows the *CO*, *PS*, and *MI* matrices obtained from the ECoG data shown in Fig. 1B. Lower row show the *CO*, *PS*, and *MI* matrices obtained from one of the 19 surrogates files in the same patient. Using this information intracortical interactions were represented in the grid according to Equation (1). In the color-grade scale, blue (0 or 0.6) represents no synchronization and red (1) perfect synchronization.

Supplementary Figure 2: *CO* statistics. $\bar{s}$ (left panel) and $\bar{v}$ (right panel) for each of the original ECoG (solid circles) and its corresponding surrogates (squares). Surrogates are represented as mean (solid squares) and standard deviation (error bars). a.u. stands for arbitrary units.

Supplementary Figure 3: Phase synchronization (*PS*) statistics. $\bar{s}$ (left panel) and $\bar{v}$ (right panel) for each of the original ECoGs (solid circles) and its corresponding surrogates. Surrogates are represented as mean (solid squares) and standard deviation (error bars). a. u. stands for arbitrary units.

Supplementary Figure 4: Mutual information (*MI*) statistics. $\bar{s}$ (left panel) and $\bar{v}$ (right panel) for each of the original ECoGs (solid circles) and its corresponding surrogates. Surrogates are represented as mean (solid squares) and standard deviation (error bars). a. u. stands for arbitrary units.

Supplementary Figure 5: z-score in $\bar{s}$ (left panel) and $\bar{v}$ (right panel). *CO* (solid circles), *PS* (empty squares), and *MI* (solid diamonds). Dashed black line in each panel marks the 1.96 threshold for a 95% confidence interval. A logarithmic scale has been used in the z-score axis.

This material is available as part of the online article from: http://www.blackwell-synergy.com/doi/abs/10.1111/j.1528-1167.2007.01266.x

(This link will take you to the article abstract).

Please note: Blackwell Publishing is not responsible for the content or functionality of any supplementary materials supplied by the authors. Any queries (other than missing material) should be directed to the corresponding author for the article.